

Stopping Rules for Algebraic Iterative Reconstruction Methods in Computed Tomography

Per Christian Hansen, Jakob Sauer Jørgensen, Peter Winkel Rasmussen
Department of Applied Mathematics and Computer Science
Technical University of Denmark, Kgs. Lyngby, Denmark
ORCID 0000-0002-7333-7216, 0000-0001-9114-754X, 0000-0002-0823-0316
Email {pcha, jakj, pwra}@dtu.dk

Abstract—Algebraic models for the reconstruction problem in X-ray computed tomography (CT) provide a flexible framework that applies to many measurement geometries. For large-scale problems we need to use iterative solvers, and we need stopping rules for these methods that terminate the iterations when we have computed a satisfactory reconstruction that balances the reconstruction error and the influence of noise from the measurements. Many such stopping rules are developed in the inverse problems communities, but they have not attained much attention in the CT world. The goal of this paper is to describe and illustrate four stopping rules that are relevant for CT reconstructions.

Index Terms—tomographic reconstruction, iterative methods, stopping rules, semi-convergence

I. INTRODUCTION

This paper considers large-scale methods for computed tomographic (CT) based on a discretization of the problem followed by solving the system of linear equations by means of an iterative solver. These methods are quite generic in the sense that they do not assume any specific scanning geometry, and they tend to produce good reconstructions with few artifacts in the case of limited-data and/or limited-angle problems.

In CT, a forward projection maps the object to the data in the form of projections of the object onto the detector planes for various scan positions. In the case of parallel-beam CT the forward projection is known as the Radon transform [21].

In practise, data consists of noisy measurements of the attenuation of the X-rays that pass through the object. The discretization of the reconstruction problem takes the form

$$\mathbf{A} \mathbf{x} \approx \mathbf{b}, \quad \mathbf{b} = \mathbf{A} \bar{\mathbf{x}} + \mathbf{e}, \quad (1)$$

where the “system matrix” $\mathbf{A} \in \mathbb{R}^{m \times n}$ is a discretization of the forward projector, $\mathbf{b} \in \mathbb{R}^m$ is a vector with the measured data, and $\mathbf{x} \in \mathbb{R}^n$ is a vector that holds the pixels of the reconstructed image of the object’s interior. Moreover, $\bar{\mathbf{x}}$ represents the exact object and \mathbf{e} represents the measurement noise. A number of discretization schemes are available for computing the matrix \mathbf{A} , see, e.g., [15], [17].

There are no restrictions on the dimensions m and n of the matrix \mathbf{A} ; both over-determined and under-determined systems

are common, depending on the measurement setup. The matrix \mathbf{A}^T represents the so-called back projector which maps the data back onto the solution domain [21]; it plays a central role in filtered back projection and similar methods.

In large-scale CT problems, the matrix \mathbf{A} – in spite of the fact that it is sparse – is often too large to store explicitly. For this reason we must use iterative solvers that only access the matrix via functions that compute the multiplications with \mathbf{A} and \mathbf{A}^T in a matrix-free fashion, often using GPUs or other hardware accelerators. In CT these iterative solvers are collectively referred to as *algebraic iterative reconstruction methods* which includes well-known methods such as ART [11] and SIRT (also known as SART) [3].

Common for all these methods is that they, from an initial vector $\mathbf{x}^{(0)}$ (often the zero vector) produce a sequence of iteration vectors $\mathbf{x}^{(k)}$, $k = 1, 2, \dots$ which, in the ideal situation, converge to the ground truth $\bar{\mathbf{x}}$. In practise, however, when noise is present in the measured data we experience a phenomenon called *semi-convergence*:

- During the initial iterations, the iteration vector $\mathbf{x}^{(k)}$ approaches the desired but un-obtainable ground truth $\bar{\mathbf{x}}$.
- During later iterations, $\mathbf{x}^{(k)}$ converges to the undesired noisy solution associated with the particular iterative method (e.g., $\mathbf{A}^{-1}\mathbf{b}$ if the system matrix is invertible).

This is illustrated in Fig. 1 which shows the error history, i.e., the reconstruction error $\|\mathbf{x}^{(k)} - \bar{\mathbf{x}}\|_2$ versus the number of iterations k , together with selected iterates $\mathbf{x}^{(k)}$ shown as images. The error history has the characteristic form associated with semi-convergence.

If we can stop the iterations just when the convergence behavior changes from the former to the latter, then we achieve an approximation to $\bar{\mathbf{x}}$ that is not too perturbed by the noise in the data. *This paper describes four such methods based on certain statistical properties of the noise.*

Sections II and III describe four state-of-the-art stopping rules as well as two methods to efficiently estimate a trace-term that is needed on some of these rules; all numerical experiments in these sections were performed by means of the AIR Tools II software package [14]. In Section IV we illustrate these techniques with a large-scale example.

This work was partially funded by a Villum Investigator grant (no. 25893) from The Villum Foundation.

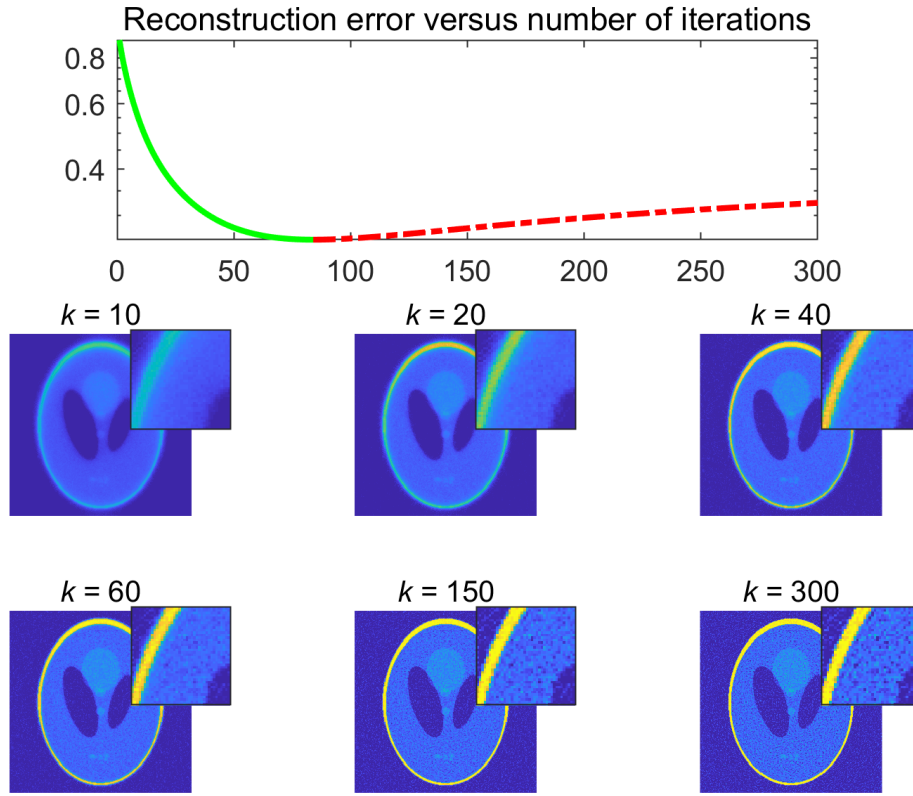


Fig. 1. Illustration of semi-convergence for Landweber’s method applied to a small noisy test problem. Top: the error history, i.e., the reconstruction error $\|\mathbf{x}^{(k)} - \bar{\mathbf{x}}\|_2$ as a function of the number of iterations k . The solid green line shows the part where $\mathbf{x}^{(k)}$ approaches $\bar{\mathbf{x}}$ while the red dash-dotted line shows the part where $\mathbf{x}^{(k)}$ becomes dominated by the noise. Bottom: selected iterations with inserts that zoom in on a small region; the increasing amount of noise is clearly visible.

II. FOUR STOPPING RULES

Our stopping rules apply to methods of the general form

$$\mathbf{x}^{(k+1)} = \mathbf{x}^{(k)} + \mathbf{D} \mathbf{A}^T \mathbf{M} (\mathbf{b} - \mathbf{A} \mathbf{x}^{(k)}), \quad (2)$$

where different choices of the diagonal matrices \mathbf{D} and \mathbf{M} lead to different methods – see, e.g., [5] for an overview. To simplify the presentation, we focus on the simple case where \mathbf{D} and \mathbf{M} are identity matrices, in which case we obtain *Landweber’s method* (which is equivalent to the steepest descent method applied to the least squares problem):

Landweber’s method

$\mathbf{x}^{(0)}$ = initial vector

for $k = 0, 1, 2, \dots$

$$\mathbf{x}^{(k+1)} = \mathbf{x}^{(k)} + \omega \mathbf{A}^T (\mathbf{b} - \mathbf{A} \mathbf{x}^{(k)})$$

end

We will frequently refer to the *residual* for the k th iterate, defined as the vector

$$\mathbf{r}^{(k)} = \mathbf{b} - \mathbf{A} \mathbf{x}^{(k)}, \quad k = 1, 2, 3, \dots \quad (3)$$

Moreover, after a bit of algebraic manipulations it turns out that we can write the k th iteration vector as

$$\mathbf{x}^{(k)} = \sum_{j=0}^{k-1} (\mathbf{I} - \omega \mathbf{A}^T \mathbf{A})^j \omega \mathbf{A}^T \mathbf{b} = \mathbf{A}_k^\# \mathbf{b}, \quad (4)$$

which defines the matrix $\mathbf{A}_k^\#$ such that we can write the k th iterate as $\mathbf{x}^{(k)} = \mathbf{A}_k^\# \mathbf{b}$. This is convenient as a theoretical tool, but $\mathbf{A}_k^\#$ is never computed explicitly.

To set the stage, we need to introduce a small amount of statistical framework and notation. We will often need the exact *noise-free data* that corresponds to the ground truth image, and we write

$$\bar{\mathbf{b}} = \mathbf{A} \bar{\mathbf{x}}. \quad (5)$$

We can then write the measured data as $\mathbf{b} = \bar{\mathbf{b}} + \mathbf{e}$. The elements of the noise vector \mathbf{e} are random variables, i.e., their values depend on a set of well-defined random events. The vector of expected values $\mathcal{E}(\mathbf{e})$ and the covariance matrix $\text{Cov}(\mathbf{e})$ are defined as

$$\mathcal{E}(\mathbf{e}) = \begin{pmatrix} \mathcal{E}(e_1) \\ \mathcal{E}(e_2) \\ \vdots \end{pmatrix}, \quad (6)$$

$$\text{Cov}(\mathbf{e}) = \mathcal{E} \left((\mathbf{e} - \mathcal{E}(\mathbf{e})) (\mathbf{e} - \mathcal{E}(\mathbf{e}))^T \right). \quad (7)$$

To simplify our discussion and make the ideas clearer, throughout this section we will restrict our analysis to *white Gaussian noise* with zero mean:

$$\mathcal{E}(e) = \mathbf{0}, \quad \text{Cov}(e) = \eta^2 \mathbf{I}, \quad \mathcal{E}(\|e\|_2^2) = m \eta^2, \quad (8)$$

where η is the standard deviation of the noise and m is the number of elements in e . Noise in tomographic problems is rarely strictly Gaussian, but sometimes this is a reasonable assumption.

A. Fitting to the Noise Level

Our description of this stopping rule is based on [15, §11.2.3]. A simple idea is to choose the number of iterations k such that the residual $\mathbf{q}^{(k)}$ is “of the same size” as the noise vector e . Specifically, such that $\|\mathbf{q}^{(k)}\|_2$ approximates the expected value $\mathcal{E}(\|e\|_2)$ of the latter:

$$\|\mathbf{q}^{(k)}\|_2 \approx \eta \sqrt{m}. \quad (9)$$

In the literature this is referred to as the *discrepancy principle* [6]. Since $\|\mathbf{q}^{(k)}\|_2$ takes discrete values for $k = 1, 2, 3, \dots$ we cannot expect to find a k such that the above holds with equality.

It is common to include a constant τ slightly larger than 1, say, $\tau = 1.02$, such that the above condition takes the form $\|\mathbf{q}^{(k)}\|_2 \leq \tau \eta \sqrt{m}$. This constant can be useful as a “safety factor” when we have only a rough estimate of the noise.

If we replace $\mathbf{x}^{(k)}$ with the ground truth $\bar{\mathbf{x}}$ then the residual is $\mathbf{b} - \mathbf{A} \bar{\mathbf{x}} = e$ and the residual norm obviously equals $\|e\|_2$. However, this is not a sound statistical argument that the norm of the residual $\mathbf{q}^{(k)}$ in Eq. (3) should be equal to $\|e\|_2$ for the optimal iterate $\mathbf{x}^{(k)}$.

Here we present an alternative that is based on statistical principles. To motivate this stopping rule, we split the residual vectors as follows:

$$\begin{aligned} \mathbf{q}^{(k)} &= \mathbf{b} - \mathbf{A} \mathbf{x}^{(k)} = \mathbf{b} - \mathbf{A} \mathbf{A}_k^\# \mathbf{b} \\ &= (\mathbf{I} - \mathbf{A} \mathbf{A}_k^\#) \bar{\mathbf{b}} + (\mathbf{I} - \mathbf{A} \mathbf{A}_k^\#) e. \end{aligned}$$

The heuristic insight is then as follows:

- When k is too small then $\mathbf{A} \mathbf{x}^{(k)}$ is not a good approximation the exact data $\bar{\mathbf{b}}$. Hence, the residual $\mathbf{q}^{(k)}$ is dominated by $(\mathbf{I} - \mathbf{A} \mathbf{A}_k^\#) \bar{\mathbf{b}}$ and $\|(\mathbf{I} - \mathbf{A} \mathbf{A}_k^\#) \bar{\mathbf{b}}\|_2$ is larger than $\|(\mathbf{I} - \mathbf{A} \mathbf{A}_k^\#) e\|_2$.
- When k is “just about right” then $\mathbf{A} \mathbf{x}^{(k)}$ approximates $\bar{\mathbf{b}}$ as well as possible; the norm $\|(\mathbf{I} - \mathbf{A} \mathbf{A}_k^\#) \bar{\mathbf{b}}\|_2$ has now become smaller and it is of the same size as the norm $\|(\mathbf{I} - \mathbf{A} \mathbf{A}_k^\#) e\|_2$.
- When k is too large then the residual $\mathbf{q}^{(k)}$ is dominated by the noise component $(\mathbf{I} - \mathbf{A} \mathbf{A}_k^\#) e$, and therefore $\|(\mathbf{I} - \mathbf{A} \mathbf{A}_k^\#) e\|_2$ dominates the residual norm.

According to these observations we should therefore choose k such that $\|(\mathbf{I} - \mathbf{A} \mathbf{A}_k^\#) \bar{\mathbf{b}}\|_2 \approx \|(\mathbf{I} - \mathbf{A} \mathbf{A}_k^\#) e\|_2$. Unfortunately both these are unknown.

The above heuristic reasoning has been formalized in [13], [18] and [25], and we will summarize the main results as they

apply here. The key points are that $\|(\mathbf{I} - \mathbf{A} \mathbf{A}_k^\#) \bar{\mathbf{b}}\|_2$ is an approximation to the prediction error $\|(\mathbf{I} - \mathbf{A} \mathbf{A}_k^\#) \mathbf{b}\|_2$ and that

$$\mathcal{E}(\|(\mathbf{I} - \mathbf{A} \mathbf{A}_k^\#) e\|_2^2) = \eta^2 (m - t_k)$$

in which

$$t_k = \text{trace}(\mathbf{A} \mathbf{A}_k^\#). \quad (10)$$

Hence, at the optimal k we have

$$\mathcal{E}(\|\mathbf{q}^{(k)}\|_2^2) \approx \eta^2 (m - t_k). \quad (11)$$

Here, k is “optimal” in the sense that it is the largest iteration number for which we cannot reject $\mathbf{x}^{(k)}$ – computed from the noisy data \mathbf{b} – as a possible solution to the noise-free system, cf. [25, p. 93].

The real number $m - t_k$ is sometimes referred to as the effective (or equivalent) degrees of freedom [27] in the residual. An exact computation of t_k is cumbersome for most methods, but it can be approximated quite efficiently as described in §III. We have thus arrived at the following “fit-to-noise-level” (FTNL) stopping rule where, again, we include the “safety factor” τ :

Stop rule: FTNL

Stop at the smallest k

$$\text{for which } \|\mathbf{q}^{(k)}\|_2 \leq \tau \eta \sqrt{m - t_k}.$$

Example 1. We illustrate the FTNL “fit-to-noise-level” stopping rule with two small parallel-beam CT problems with image size 64×64 and 91 detector pixels. The projection angles are, respectively, $3^\circ, 6^\circ, 9^\circ, \dots, 180^\circ$ (giving an over-determined system) and $8^\circ, 16^\circ, 24^\circ, \dots, 180^\circ$ (giving an under-determined system). In both cases we removed zero rows from the system matrix.

We used Landweber’s method to solve these two problems. Figure 2 shows the reconstruction errors $\|\mathbf{x}^{(k)} - \bar{\mathbf{x}}\|_2$ and the norms $\|\mathbf{q}^{(k)}\|_2$ versus k , together with the threshold $\eta \sqrt{m}$ and the function $\eta \sqrt{m - t_k}$, i.e., here we use $\tau = 1$. The graphs confirm the monotonic decrease of the residual norm. For both problems, the “fit-to-noise-level” stopping rule terminates the iterations close to the optimal number of iterations. A stopping rule involving $\eta \sqrt{m}$, on the other hand, would terminate the iterations much too early. \square

B. Minimization of the Prediction Error – UPRE

The key idea is to find the number of iterations that minimizes the prediction error, i.e., the difference between the noise-free data $\bar{\mathbf{b}} = \mathbf{A} \bar{\mathbf{x}}$ and the predicted data $\mathbf{A} \mathbf{x}^{(k)}$. Statisticians refer to various measures of this difference as the predictive risk, and the resulting method for choosing k is often called the *unbiased predictive risk estimation (UPRE)* method.

Here we present the results specifically in the framework of iterative reconstruction methods and using the matrix $\mathbf{A}_k^\#$ defined in Eq. (4). Following [26, §7.1], where all the details

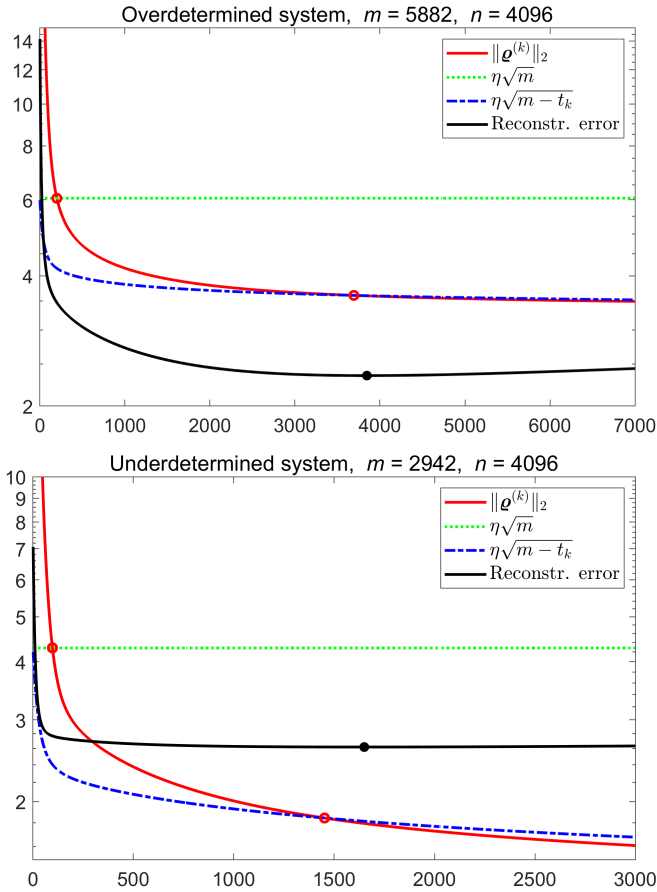


Fig. 2. Illustration of the FTNL stopping rule for Landweber's method, with two parallel-beam tomographic problems. The smallest reconstruction error is marked with the black dot, and the residual norms that satisfies the stopping rules are marked with red circles. The FTNL rule works well, while stopping at that k for which $\|\mathbf{q}^{(k)}\|_2 \approx \eta\sqrt{m}$ terminates the iterations much too early.

can be found, the expected squared norm of the prediction error (the risk) is

$$\mathcal{E}(\|\bar{\mathbf{b}} - \mathbf{A}\mathbf{x}^{(k)}\|_2^2) = \|(I - \mathbf{A}\mathbf{A}_k^\#)\bar{\mathbf{b}}\|_2^2 + \eta^2 \text{trace}((\mathbf{A}\mathbf{A}_k^\#)^2)$$

while the expected squared norm of the residual can be written as

$$\mathcal{E}(\|\mathbf{b} - \mathbf{A}\mathbf{x}^{(k)}\|_2^2) = \|(I - \mathbf{A}\mathbf{A}_k^\#)\mathbf{b}\|_2^2 + \eta^2 \text{trace}((\mathbf{A}\mathbf{A}_k^\#)^2) - 2\eta^2 \text{trace}(\mathbf{A}\mathbf{A}_k^\#) + \eta^2 m .$$

Combining these two equations we can eliminate one of the trace terms and arrive at the following expression for the risk:

$$\mathcal{E}(\|\bar{\mathbf{b}} - \mathbf{A}\mathbf{x}^{(k)}\|_2^2) = \mathcal{E}(\|\mathbf{b} - \mathbf{A}\mathbf{x}^{(k)}\|_2^2) + 2\eta^2 \text{trace}(\mathbf{A}\mathbf{A}_k^\#) - \eta^2 m .$$

Substituting the actual squared residual norm $\|\mathbf{q}^{(k)}\|_2^2 = \|\mathbf{b} - \mathbf{A}\mathbf{x}^{(k)}\|_2^2$ for its expected value, we thus define the UPRE risk as a function of k :

$$U^{(k)} = \|\mathbf{q}^{(k)}\|_2^2 + 2\eta^2 t_k - \eta^2 m \quad (12)$$

with t_k given by (10). A minimizer of $U^{(k)}$ will then give an approximation to a minimizer of the prediction error. We note that $U^{(k)}$ may not have a unique minimizer, and we therefore choose the smallest k at which $U^{(k)}$ has a local minimum. Thus we arrive at the following stopping rule:

Stop rule: UPRE

$$\text{Minimize } U^{(k)} = \|\mathbf{q}^{(k)}\|_2^2 + 2\eta^2 t_k - \eta^2 m .$$

C. Another Rule Based on the Prediction Error – GCV

The above UPRE stopping rule depends on an estimate of the standard deviation η of the noise – which may or may not be a problem in practise. We shall now describe an alternative method for minimization of the prediction error, derived by Wahba [27], that does not depend on knowledge of η .

The outset for this method is the principle of cross validation. Assume that we remove the i th element b_i from the right-hand side (the noisy data), compute a reconstruction $\mathbf{x}_{[i]}^{(k)}$, and then use this reconstruction to compute a prediction $\hat{b}_i = \mathbf{r}_i^T \mathbf{x}_{[i]}^{(k)}$ of the missing data b_i , where

$$\mathbf{r}_i^T = \mathbf{A}(i, :) = i\text{th row of } \mathbf{A} .$$

The goal would then be to choose the number of iterations k that minimizes the mean of all the squared prediction errors:

$$\hat{G}^{(k)} = \frac{1}{m} \sum_{i=1}^m (b_i - \hat{b}_i)^2 = \frac{1}{m} \sum_{i=1}^m \left(b_i - \mathbf{r}_i^T \mathbf{x}_{[i]}^{(k)} \right)^2 .$$

Then it is proved in [27, Thm. 4.2.1] that we can avoid the vectors $\mathbf{x}_{[i]}^{(k)}$ and write $\hat{G}^{(k)}$ directly in terms of $\mathbf{x}^{(k)}$:

$$\hat{G}^{(k)} = \frac{1}{m} \sum_{i=1}^m \left(\frac{b_i - \mathbf{r}_i^T \mathbf{x}^{(k)}}{1 - \alpha_i^{(k)}} \right)^2, \quad (13)$$

where $\alpha_i^{(k)}$ is the i th diagonal element of the matrix product $\mathbf{A}\mathbf{A}_k^\#$ associated with $\mathbf{x}^{(k)}$.

At this stage, recall that the 2-norm is invariant under an orthogonal transformation, of which a permutation is a special case. Specifically, if \mathbf{Q} is an orthogonal matrix then

$$\|\mathbf{Q}(\mathbf{A}\mathbf{x} - \mathbf{b})\|_2 = \|\mathbf{A}\mathbf{x} - \mathbf{b}\|_2$$

which means that the reconstruction $\mathbf{x}^{(k)}$ is invariant to such a transformation. Unfortunately it can be proved [27] that the minimizer of $\hat{G}^{(k)}$ is not invariant to an orthogonal transformation of the data. In particular, it is inconvenient that a stopping rule based on $\hat{G}^{(k)}$ would produce a k that depends on the particular ordering of the data.

The *generalized cross validation (GCV)* method circumvents this problem by replacing all $\alpha_i^{(k)}$ with their average

$$\mu^{(k)} = \frac{1}{m} \sum_{i=1}^m \alpha_i^{(k)} = \frac{1}{m} \text{trace}(\mathbf{A}\mathbf{A}_k^\#) = \frac{t_k}{m} ,$$

leading to the modified measure

$$\begin{aligned}\tilde{G}^{(k)} &= \frac{1}{m} \frac{1}{(1 - \mu^{(k)})^2} \sum_{i=1}^m (b_i - \mathbf{r}_i^T \mathbf{x}^{(k)})^2 \\ &= \frac{\|\mathbf{b} - \mathbf{A} \mathbf{x}^{(k)}\|_2^2}{m(1 - t_k/m)^2} = m \frac{\|\boldsymbol{\rho}^{(k)}\|_2^2}{(m - t_k)^2}.\end{aligned}\quad (14)$$

The minimizer of $\tilde{G}^{(k)}$ is, of course, independent of the factor m and hence we choose to define the GCV risk as a function of k as

$$G^{(k)} = \frac{\|\boldsymbol{\rho}^{(k)}\|_2^2}{(m - t_k)^2}.\quad (15)$$

We have thus arrived at the following η -free stopping rule where again, in practice, we need to estimate the quantity t_k :

Stop rule: GCV

$$\text{Minimize } G^{(k)} = \|\boldsymbol{\rho}^{(k)}\|_2^2 / (m - t_k)^2.$$

The above presentation follows [27, §4.2–3]. A different derivation of the GCV method was presented in [10]; here the coordinate system for \mathbb{R}^m is rotated such that the corresponding influence matrix becomes a circulant matrix with identical elements along all its diagonals. This approach leads to the same GCV risk $G^{(k)}$ as above.

Perhaps the most important property of the GCV stopping rule is that the value of k which minimizes $G^{(k)}$ in (15) is also an estimate of the value that minimizes the prediction error. Specifically, if k_{GCV} minimizes the GCV risk $G^{(k)}$ and k_{PRE} minimizes the prediction error $\|\bar{\mathbf{b}} - \mathbf{A} \mathbf{x}^{(k)}\|_2^2$, then it is shown in [27, §4.4] that

$$\begin{aligned}\mathcal{E}(\|\bar{\mathbf{b}} - \mathbf{A} \mathbf{x}^{(k_{\text{GCV}})}\|_2^2) &\rightarrow \mathcal{E}(\|\bar{\mathbf{b}} - \mathbf{A} \mathbf{x}^{(k_{\text{PRE}})}\|_2^2) \\ &\text{for } m \rightarrow \infty.\end{aligned}$$

The UPRE and GCV stopping rules have the slight inconvenience that we need to take at least one iteration too many in order to detect a minimum of $U^{(k)}$ and $G^{(k)}$, respectively. In practise, this is not really a problem. For tomography problems the iteration vector $\mathbf{x}^{(k)}$ does not change very much from one iteration to the next, and hence the minimum of the error history $\|\bar{\mathbf{x}} - \mathbf{x}^{(k)}\|_2$ is usually very flat. Hence it hardly makes any difference if we implement the UPRE and GCV stopping rules such that we terminate the method one iteration (or a few iterations) after the actual minimum of $U^{(k)}$ or $G^{(k)}$.

Example 2. We illustrate the UPRE and GCV stopping rules applied to Landweber’s method with the two CT problems from Example 1. In both cases we removed zero rows from the system matrix. Figure 3 shows $U^{(k)}$ and $G^{(k)}$ from Eqs. (12) and (15) versus k , together with the error histories. The two stopping rules terminate the iterations at approximately the same number of iterations – not too far from the minimum of the error history. Note how flat the error history is: in practise it makes no difference if we terminate the iterations exactly at the minimum of $U^{(k)}$ and $G^{(k)}$ or a few iterations later. \square

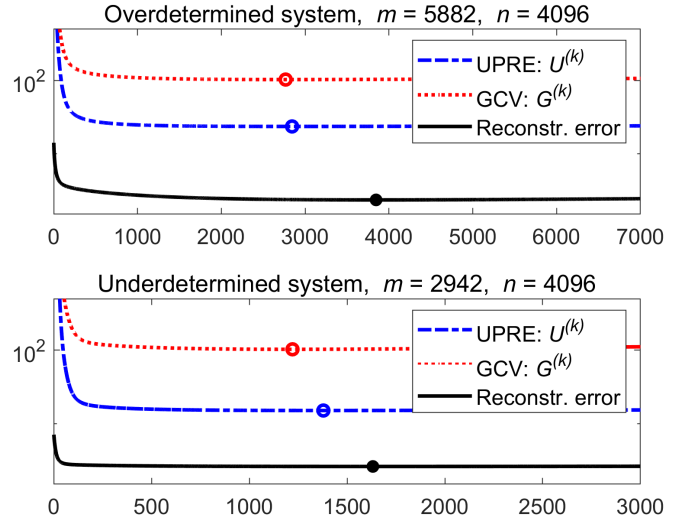


Fig. 3. Illustration of the UPRE and GCV stopping rules for Landweber’s method applied to the two parallel-beam CT problems in Example 1 and 2.

D. Stopping When All Information is Extracted — NCP

The above stopping rules include the trace term t_k in Eq. (10). This term can be estimated at additional cost as discussed in §III below, but it is also worthwhile to consider a stopping rule that needs neither the trace term t_k nor the standard deviation η of the noise. The so-called NCP criterion from [16] and [23] is one such method. The considerations that underly this method are as follows:

- 1) noisy data only contain partial information about the reconstruction,
- 2) in each iteration we extract more information from the data, and
- 3) eventually we have extracted all the available information in the noisy data.

Therefore we want to monitor the properties of the residual vector. During the initial iterations we have not yet extracted all information present in the data and the residual still resembles a meaningful signal, while at some stage – when all information is extracted – the residual starts to appear like noise. When we iterate beyond this point, we solely extract noise from the data (we “fit the noise”) and the residual vector will appear as filtered noise where some of the noise’s spectral components are removed.

To formalize this approach, in the white-noise setting of this presentation, we need a computational approach to answering the questions: when does the residual vector look the most like white noise? To answer this question, statisticians introduced the so-called normalized cumulative periodogram.

In the terminology of signal processing, a periodogram is identical to a discrete power spectrum defined as the squared absolute values of the discrete Fourier coefficients. Hence the periodogram for an arbitrary vector $\mathbf{v} \in \mathbb{R}^m$ is given by

$$\hat{p}_i = |\hat{v}_i|^2, \quad i = 1, 2, \dots, q, \quad \hat{\mathbf{v}} = \text{DFT}(\mathbf{v}).\quad (16)$$

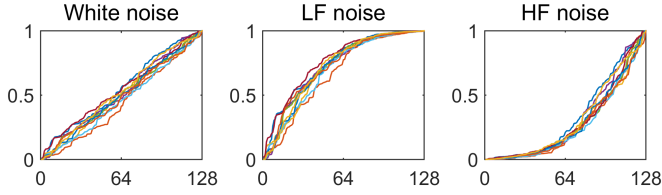


Fig. 4. Illustration of NCP vectors $\mathbf{c}(\mathbf{v}) \in \mathbb{R}^{256}$ for vectors \mathbf{v} that are white noise (left), dominated by low-frequency components (middle), and dominated by high-frequency components (right).

Here, DFT denotes the discrete Fourier transform (computed by means of the FFT algorithm) and $q = \lfloor m/2 \rfloor$ denotes the largest integer such that $q \leq m/2$. The reason for including only about half of the Fourier coefficients in the periodogram/power spectrum is that the DFT of a real vector is symmetric about its midpoint. We then define the corresponding *normalized cumulative periodogram (NCP)* for the vector \mathbf{v} as the vector $\mathbf{c}(\mathbf{v})$ of length q with elements, for $j = 1, 2, \dots, q$,

$$c_j(\mathbf{v}) = \frac{\widehat{p}_2 + \dots + \widehat{p}_{j+1}}{\widehat{p}_2 + \dots + \widehat{p}_{q+1}} = \frac{\|\widehat{\mathbf{v}}_{2:j+1}\|_2^2}{\|\widehat{\mathbf{v}}_{2:q+1}\|_2^2}. \quad (17)$$

White noise is characterized by having a flat power spectrum (similar to white light having equal amounts of all colors), and thus the expected value of its power spectrum components is a constant independent of i . Consequently, the expected value of the NCP for a white-noise vector \mathbf{v}_w is the vector

$$\mathcal{E}(\mathbf{c}(\mathbf{v}_w)) = \mathbf{c}_w = \left(\frac{1}{q}, \frac{2}{q}, \dots, 1 \right).$$

How much a given vector \mathbf{v} deviates from being white noise can be measured by the deviation of the corresponding $\mathbf{c}(\mathbf{v})$ from \mathbf{c}_w , e.g., as measured by the norm $\|\mathbf{c}(\mathbf{v}) - \mathbf{c}_w\|_2$.

Example 3. Figure 4 illustrates the appearance of NCP vectors $\mathbf{c}(\mathbf{v})$ for vectors \mathbf{v} of length $m = 256$ with different spectra. The completely flat spectrum for white noise corresponds to a straight line from $(0,0)$ to $(q,1)$ with $q = \lfloor 256/2 \rfloor = 128$. The left plot shows NCPs for 10 random realizations of white noise, and they are all close to the ideal white-noise NCP \mathbf{c}_w . The middle and right plots show NCPs for random vectors that are dominated by low-frequency and high-frequency components, respectively; their systematic deviation from \mathbf{c}_w is obvious. \square

To utilize the NCP framework in the algebraic iterative methods for tomographic reconstruction, a first idea might be to terminate the iterations when the deviation measured by $\|\mathbf{c}(\mathbf{q}^{(k)}) - \mathbf{c}_w\|_2$ exhibits a minimum. However, this would be a bit naive since the residual vector does not really correspond to a 1D signal of length m . Rather, the right-hand side \mathbf{b} consists of a number of projections, one for each angle of the measurements – and the residual vector inherits this structure. Hence, a better approach is to apply an NCP analysis to each projection’s residual, and then combine this information into a simple measure.

Depending on the CT scanner, each projection is either a 1D or 2D image, when we perform 2D and 3D reconstructions,

respectively. To simplify our presentation, we assume that our data consists of m_θ 1D projections, one for each projection angle $\theta_1, \theta_2, \dots, \theta_{m_\theta}$. We also assume that the data are organized such that we can partition the right-hand side \mathbf{b} and the residual vector into m_θ sub-vectors,

$$\mathbf{b} = \begin{pmatrix} \mathbf{b}_1 \\ \mathbf{b}_2 \\ \vdots \\ \mathbf{b}_{m_\theta} \end{pmatrix}, \quad \mathbf{q}^{(k)} = \begin{pmatrix} \mathbf{q}_1^{(k)} \\ \mathbf{q}_2^{(k)} \\ \vdots \\ \mathbf{q}_{m_\theta}^{(k)} \end{pmatrix}, \quad (18)$$

with each sub-vector corresponding to a single 1D projection. Now define the corresponding quantities

$$\nu_\ell^{(k)} = \|\mathbf{c}(\mathbf{q}_\ell^{(k)}) - \mathbf{c}_w\|_2, \quad \ell = 1, 2, \dots, m_\theta \quad (19)$$

that measure the deviation of each residual sub-vector from being white noise. Then for the k th iteration we propose to measure the residual’s deviation from being white noise by averaging the above quantities, i.e., by means of the “NCP-number”

$$N^{(k)} = \frac{1}{m_\theta} \sum_{\ell=1}^{m_\theta} \nu_\ell^{(k)}. \quad (20)$$

This multi-1D approach for 2D reconstruction problems leads to the following stopping rule:

Stop rule: NCP

Minimize $N^{(k)} = \frac{1}{m_\theta} \sum_{\ell=1}^{m_\theta} \|\mathbf{c}(\mathbf{q}_\ell^{(k)}) - \mathbf{c}_w\|_2$.

In the case of 3D reconstructions, where the data consist of a collection of 2D images, the computation of $\nu_\ell^{(k)}$ should take this into consideration. In particular we need to define the NCP vector $\mathbf{c}(\mathbf{q}_\ell^{(k)})$ when the residual sub-vector $\mathbf{q}_\ell^{(k)}$ represents an image; how to do this is explained in [16].

Similar to the previous stopping rules, in practise it is more convenient to implement the NCP stopping rule such that we terminate the iterations at the first iteration k for which $N^{(k)}$ increases. There is no theory to guarantee that $N^{(k)}$ will behave smoothly, and we occasionally see that $N^{(k)}$ exhibits a minor zig-zag behavior. Hence it may be necessary to apply the NCP stopping rule to a smoothed version of the NCP-numbers, obtained by applying a “local” low-pass filter to the $N^{(k)}$ -sequence.

Example 4. We illustrate the NCP stopping rule with a parallel-beam CT problem with image size 256×256 and with 362 detector pixels and projection angles $1^\circ, 2^\circ, \dots, 180^\circ$. The performance is shown in Fig. 5 together with surface plots of the matrix $[\mathbf{c}(\mathbf{q}_1^{(k)}), \mathbf{c}(\mathbf{q}_2^{(k)}), \dots, \mathbf{c}(\mathbf{q}_{m_\theta}^{(k)})]$ for selected iterations k . We clearly see the changing shape of the NCP vectors $\mathbf{c}(\mathbf{q}_\ell^{(k)})$ as k increases. The minimum of $N^{(k)}$ is obtained at $k_{\text{NCP}} = 179$. This is somewhat early, considering that the minimum reconstruction error is obtained at $k = 497$ iterations – but on the other hand, the reconstruction and the error changes only little between iterations 150 and 700. \square

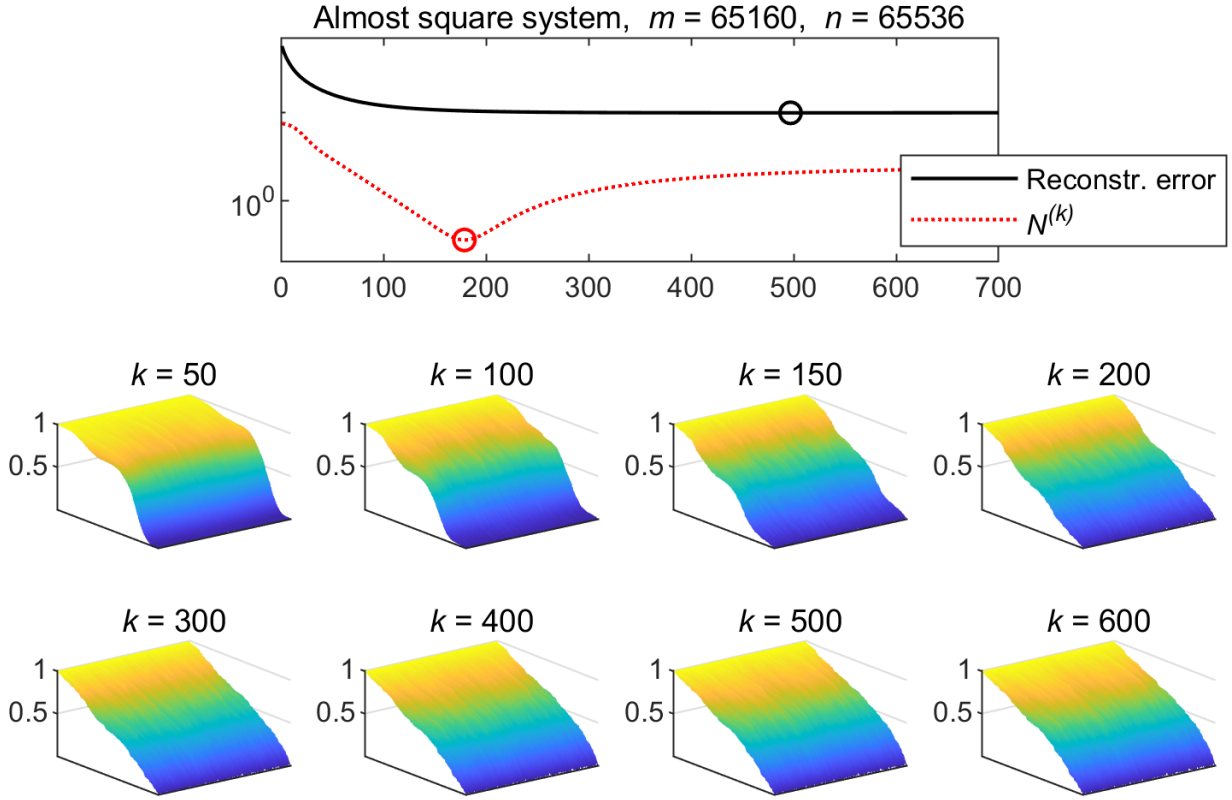


Fig. 5. Illustration of the NCP stopping rules for Landweber’s method applied to a parallel-beam test problem. We also show surface plots of the matrix $[c(\varrho_1^{(k)}), c(\varrho_2^{(k)}), \dots, c(\varrho_{m_\theta}^{(k)})]$ for selected iterations k . This stopping rule leads to a somewhat premature termination of the iterations at $k_{\text{NCP}} = 179$ (the minimum error occurs for $k = 497$ iterations), but it should be noted that the error does not change much between iterations 179 and 700.

III. ESTIMATION OF THE TRACE TERM

The FTNL, UPRE and GCV stopping rules include the term $t_k = \text{trace}(\mathbf{A} \mathbf{A}_k^\#)$. To make these methods practical to use, we need to be able to estimate this trace term efficiently, without having to compute the SVD of the system matrix \mathbf{A} or form the influence matrix $\mathbf{A} \mathbf{A}_k^\#$. The most common way to compute this estimate is via a Monte Carlo approach.

Underlying this approach is the following result from [9]. If $\bar{\mathbf{w}} \in \mathbb{R}^m$ is a random vector with elements $\bar{w}_i \sim \mathcal{N}(0, 1)$, and if $\mathbf{S} \in \mathbb{R}^{m \times m}$ is a symmetric matrix, then $\bar{\mathbf{w}}^T \mathbf{S} \bar{\mathbf{w}}$ is an unbiased estimate of $\text{trace}(\mathbf{S})$. Therefore $\bar{t}_k^{\text{est}} = \bar{\mathbf{w}}^T \mathbf{A} \mathbf{A}_k^\# \bar{\mathbf{w}}$ is an unbiased estimator of $t_k = \text{trace}(\mathbf{A} \mathbf{A}_k^\#)$.

To compute this estimate we need to compute the matrix-vector product $\mathbf{A}_k^\# \bar{\mathbf{w}}$ efficiently. Recalling the definition of $\mathbf{A}_k^\#$ in Eq. (4), this can be done simply by applying the algebraic iterative method to the system $\mathbf{A} \bar{\boldsymbol{\xi}} = \bar{\mathbf{w}}$ which, after k iterations, produces the iteration vector $\bar{\boldsymbol{\xi}}^{(k)} = \mathbf{A}_k^\# \bar{\mathbf{w}}$. The resulting estimate

$$\bar{t}_k^{\text{est}} = \bar{\mathbf{w}}^T \mathbf{A} \bar{\boldsymbol{\xi}}^{(k)} = (\mathbf{A}^T \bar{\mathbf{w}})^T \bar{\boldsymbol{\xi}}^{(k)} \quad (21)$$

is the standard Monte Carlo trace estimate from [9]. In an efficient implementation of (21) the vector $\mathbf{A}^T \bar{\mathbf{w}}$ is pre-computed and stored.

An alternative approach was presented in [24]. This approach also applies to the general method in (2) with $\mathbf{D} = \mathbf{I}$

and with a general $m \times m$ matrix \mathbf{M} (it is not required to be symmetric). When we apply such a method with an arbitrary nonzero starting vector $\boldsymbol{\xi}^{(0)}$ to the system $\mathbf{A} \boldsymbol{\xi} = \mathbf{0}$, then it follows from Eq. (4) that the iterates are

$$\boldsymbol{\xi}^{(k)} = (\mathbf{I} - \omega \mathbf{A}^T \mathbf{B} \mathbf{A})^k \boldsymbol{\xi}^{(0)} .$$

Then it is shown in [24] that if we use a random starting vector $\boldsymbol{\xi}^{(0)} = \mathbf{w} \in \mathbb{R}^n$ with elements $w_i \sim \mathcal{N}(0, 1)$, and if $\boldsymbol{\xi}^{(k)}$ denotes the corresponding iterations for the system $\mathbf{A} \boldsymbol{\xi} = \mathbf{0}$, then $\mathbf{w}^T \boldsymbol{\xi}^{(k)}$ is an unbiased estimator of $n - \text{trace}(\mathbf{A} \mathbf{A}_k^\#)$. This leads to the alternative trace estimate

$$t_k^{\text{est}} = n - \mathbf{w}^T \boldsymbol{\xi}^{(k)} . \quad (22)$$

In order to use either of these trace estimates instead of the exact t_k , we must simultaneously apply the iterative method to two right-hand sides, which essentially doubles the amount of work. The Landweber method with the two different trace estimation schemes are shown below.

If we are willing to increase the overhead further, we can compute a more robust estimate of t_k by applying the above idea to several random vectors and computing the mean or median of the t_k^{est} -values.

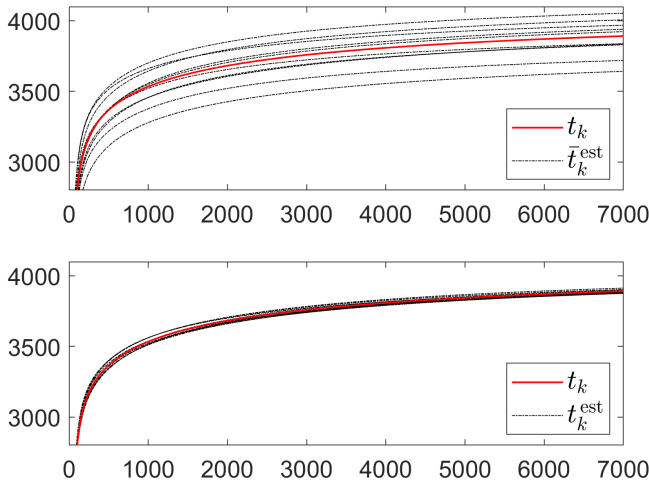


Fig. 6. Comparison of the two trace estimates \bar{t}_k^{est} and t_k^{est} for Landweber's method applied to the over-determined test problem from Example 1. The thick red line is the exact trace t_k , and the thin black lines are the trace estimates for 10 different random vectors $\bar{\mathbf{w}}$ and \mathbf{w} .

Landweber method with (21) trace estimator

$\bar{\mathbf{w}}$ = random m -vector for trace estimation
 $\mathbf{x}^{(0)}$ = initial vector
 $\bar{\boldsymbol{\xi}}^{(0)}$ = $\mathbf{0}$ initial zero vector for trace estimation
 $\mathbf{z} = \mathbf{A}^T \bar{\mathbf{w}}$
for $k = 0, 1, 2, \dots$
 $\mathbf{x}^{(k+1)} = \mathbf{x}^{(k)} + \omega \mathbf{A}^T (\mathbf{b} - \mathbf{A} \mathbf{x}^{(k)})$
 $\bar{\boldsymbol{\xi}}^{(k+1)} = \bar{\boldsymbol{\xi}}^{(k)} + \omega \mathbf{A}^T (\bar{\mathbf{w}} - \mathbf{A} \bar{\boldsymbol{\xi}}^{(k)})$
 $\bar{t}_{k+1}^{\text{est}} = \mathbf{z}^T \bar{\boldsymbol{\xi}}^{(k+1)}$ trace estimate
stopping rule goes here
end

Landweber method with (22) trace estimator

\mathbf{w} = random n -vector
 $\mathbf{x}^{(0)}$ = initial vector
 $\boldsymbol{\xi}^{(0)} = \mathbf{w}$ initial vector for for trace estimation
for $k = 0, 1, 2, \dots$
 $\mathbf{x}^{(k+1)} = \mathbf{x}^{(k)} + \omega \mathbf{A}^T (\mathbf{b} - \mathbf{A} \mathbf{x}^{(k)})$
 $\boldsymbol{\xi}^{(k+1)} = \boldsymbol{\xi}^{(k)} + \omega \mathbf{A}^T (\mathbf{0} - \mathbf{A} \boldsymbol{\xi}^{(k)})$
 $t_{k+1}^{\text{est}} = n - \mathbf{w}^T \boldsymbol{\xi}^{(k+1)}$ trace estimate
stopping rule goes here
end

Example 5. We illustrate the two trace estimates \bar{t}_k^{est} and t_k^{est} for Landweber's method applied to the over-determined test problem from Example 1. Figure 6 shows the trace estimates for 10 different realizations of the random vectors $\bar{\mathbf{w}}$ and \mathbf{w} , together with the exact trace t_k . We see that the estimate t_k^{est} , shown in the bottom plot, has the smallest variance. We

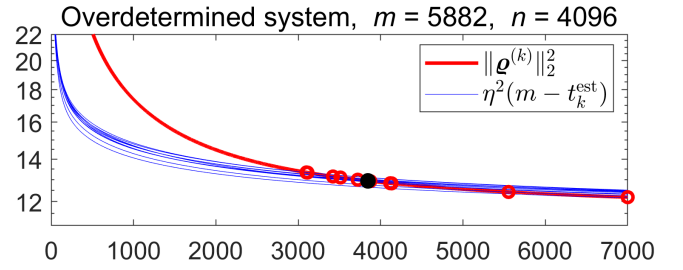


Fig. 7. Illustration of the use of the trace estimate t_k^{est} in the FTNL stopping rule for Landweber's method applied to the over-determined test problem from Examples 1. We used 10 different random vectors \mathbf{w} in (22) and the corresponding 10 intersections between $\|\mathbf{q}^{(k)}\|_2^2$ (thick red line) and $\eta^2(m - t_k^{\text{est}})$ (thin blue lines) are shown by the red circles. The black dot shows the intersection with the exact $\eta^2(m - t_k)$.

are not aware of theory that supports this observation. \square

Example 6. Continuing from the previous example, Fig. 7 illustrates the use of the trace estimate t_k^{est} in the FTNL stopping rule. To show the variability of the stopping rule we used 10 different random vectors \mathbf{w} , leading to 10 different realizations of $\eta^2(m - t_k^{\text{est}})$. Their intersections with $\|\mathbf{q}^{(k)}\|_2^2$ are shown by the red circles, corresponding to stopping the iterations at

$$k = 3100, 3112, 3421, 3512, 3722, \\ 3875, 4117, 4133, 5553, 7000.$$

The black dot marks the intersection of the exact of $\|\mathbf{q}^{(k)}\|_2^2$ with $\eta^2(m - t_k)$, corresponding to iteration $k = 3846$. \square

IV. LARGE-SCALE NUMERICAL EXAMPLE

In this section we use a simulated large-scale CT reconstruction problem to illustrate the use of the GCV and NCP stopping rules described above. We focus on an application in dynamic tomography where the time scale of the process being examined dictates the use of a small number of projections as well as short exposure times of each projection. This leads to challenging reconstruction problems where it is critical to use a stopping rules that terminates the iterations such that $\mathbf{x}^{(k)}$ is as close as possible to $\bar{\mathbf{x}}$ and without having knowledge of the noise level in the data.

Specifically we study the use of the GCV and NCP stopping rules applied to the reconstruction of a single time step in a simulation of a dynamic CT experiment. The dynamic process under study is the separation of an emulsion of oil and water in a porous rock; the components separate vigorously over time, due to the two fluids being immiscible.

The basis of our simulation is a segmentation of a nano-CT scan of a piece of chalk from the Hod field in the North Sea Basin (sample id HC #15) which was scanned, reconstructed and segmented as described in [4], [20]. A subset consisting of $200 \times 256 \times 256$ voxels is chosen for the fluid simulation. Pixels outside a radius of 124 pixels from the center axis are set to zero to form a cylinder, which is mirrored along its vertical axis to ensure that the multiphase flow simulation has periodic boundary conditions. The flow simulation is done

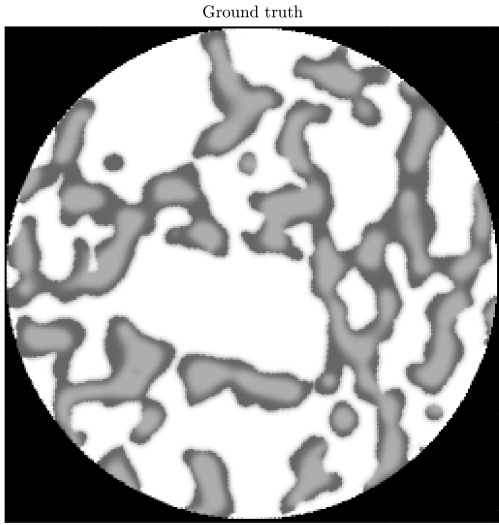


Fig. 8. A single slice of the volume being examined. White corresponds to rock while light and dark grey correspond to water and oil respectively.

with a phase-field Lattice Boltzmann method for systems that are isothermal and incompressible [7], [8]. The simulation produces phase values for each voxel that describes the fraction of oil and water in the voxel. These phase values are converted to attenuation values based on values measured in [19] where a sandstone filled with a brine and oil is imaged with X-rays at 80 keV.

Figure 8 shows a slice from a single time frame in the simulation; the rock matrix is white, the water phase is light grey, and the oil phase is dark grey. The time frame which was chosen for testing the stopping rules is fairly early in the simulation where multiple interfaces between the two fluids are present.

Forward projection: The forward projection of the volume is performed using the ASTRA toolbox with a parallel beam geometry [1], [2], [22]. We use 362 detector pixels and 360 projection angles. The forward projection in ASTRA can be considered an ideal experiment with monochromatic X-rays and infinite brilliance, i.e., without any noise.

Noise: We create noisy data from the above clean data in such a way that we emulate the noise present in X-ray tomography as a result of the finite count of photons, cf. [15, §4.4]. Specifically, if $\bar{\mathbf{b}} = \mathbf{A}\bar{\mathbf{x}}$ denotes the clean data computed by means of ASTRA, then the corresponding X-ray intensities at the detector are given by

$$\bar{I}_i = I_0 \exp(-\bar{b}_i), \quad i = 1, \dots, m,$$

where I_0 is the source's intensity. We then use \bar{I}_i as the expected value in a Poisson distribution to obtain noisy intensities

$$I_i = \mathcal{P}(\bar{I}_i) = \mathcal{P}(I_0 \exp(-\bar{b}_i)), \quad i = 1, \dots, m.$$

Finally, we convert these noisy intensities back to the noisy data vector \mathbf{b} via the relation

$$b_i = -\log(I_i/I_0), \quad i = 1, \dots, m.$$

We use three different noise levels 0.25%, 1% and 5% which visually corresponds to low, moderate and high noise. The noise level is given by

$$\rho = \frac{\|\mathbf{e}\|_2}{\|\bar{\mathbf{b}}\|_2}, \quad \mathbf{e} = \mathbf{b} - \bar{\mathbf{b}}, \quad (23)$$

where \mathbf{e} denotes the measurement error in Eq. (1). This noise does not exactly fit with the assumption of white Gaussian noise which is used for the previous derivations, but it is a good approximation to the noise present in CT experiments.

Reconstruction: We compute reconstructions from the simulated projection data with the ASTRA toolbox by using the Simultaneous Iterative Reconstruction Technique (SIRT) iterative method. This is a special case of the general method in Eq. (2) where the diagonal matrices \mathbf{D} and \mathbf{M} contain the inverse column and row sums of \mathbf{A} :

$$d_{jj} = 1 / \sum_{i=1}^m a_{ij} \quad \text{and} \quad m_{ii} = 1 / \sum_{j=1}^n a_{ij}.$$

We perform 1000 SIRT iterations and for UPRE and GCV the trace $t^{(k)}$ in $U^{(k)}$ and $G^{(k)}$ is estimated using Eq. (21). Note that only a single random vector \mathbf{w} is used to reduce computation time. This is not a concern in this specific case as the estimation of $t^{(k)}$ proved very stable for different random vectors.

The forward projection of $\mathbf{x}^{(k)}$ used in the calculation of $N^{(k)}$ is computed with ASTRA, and the remaining part of the algorithm is calculated with CuPy, a Python package which makes it possible to offload calculations to a CUDA-compatible GPU to improve the computation time of $N^{(k)}$. The vector \mathbf{v} in (16) is padded with zeros such that its length can be written in the form $n = 2^a + 3^b + 5^c + 7^d$ as this substantially speeds up the calculation when the DFT is calculated with CUDA.

Results: As previously mentioned, we reconstruct the data at three different noise levels. Moreover, we subsample the number of projections used for the reconstruction such that it is performed with 360, 120 and 45 projection angles. This leads to 9 different data sets.

Figure 9 shows graphs of $\|\mathbf{g}^{(k)}\|_2$, $\tau \eta \sqrt{m - t_k}$ (called FTNL), $U^{(k)}$, $G^{(k)}$, $N^{(k)}$ and $\|\mathbf{x}^{(k)} - \bar{\mathbf{x}}\|_2$ along with their local minima. In general we see that the FTNL and UPRE stopping rules perform well in this simulated example; but they depend on knowledge of the noise level η which is rarely known for real data. An advantage of the GCV and NCP stopping rules is that they do not rely on an estimate of η . GCV performs well in the case with 1% and 5% noise, but it overestimates the number of iterations with the small noise level $\rho = 0.25\%$. The NCP stopping rule is also a robust method and it performs well for all noise levels. It is worth noting that the reconstruction error is very flat for this noise level, which means the exact amount of iterations used is less critical.

Figure 10 shows the effect of semi-convergence on the data set when it is reconstructed with $N_{\text{proj}} = 360$ and $\rho = 1.00\%$. A single slice of the reconstruction is shown in all subfigures.

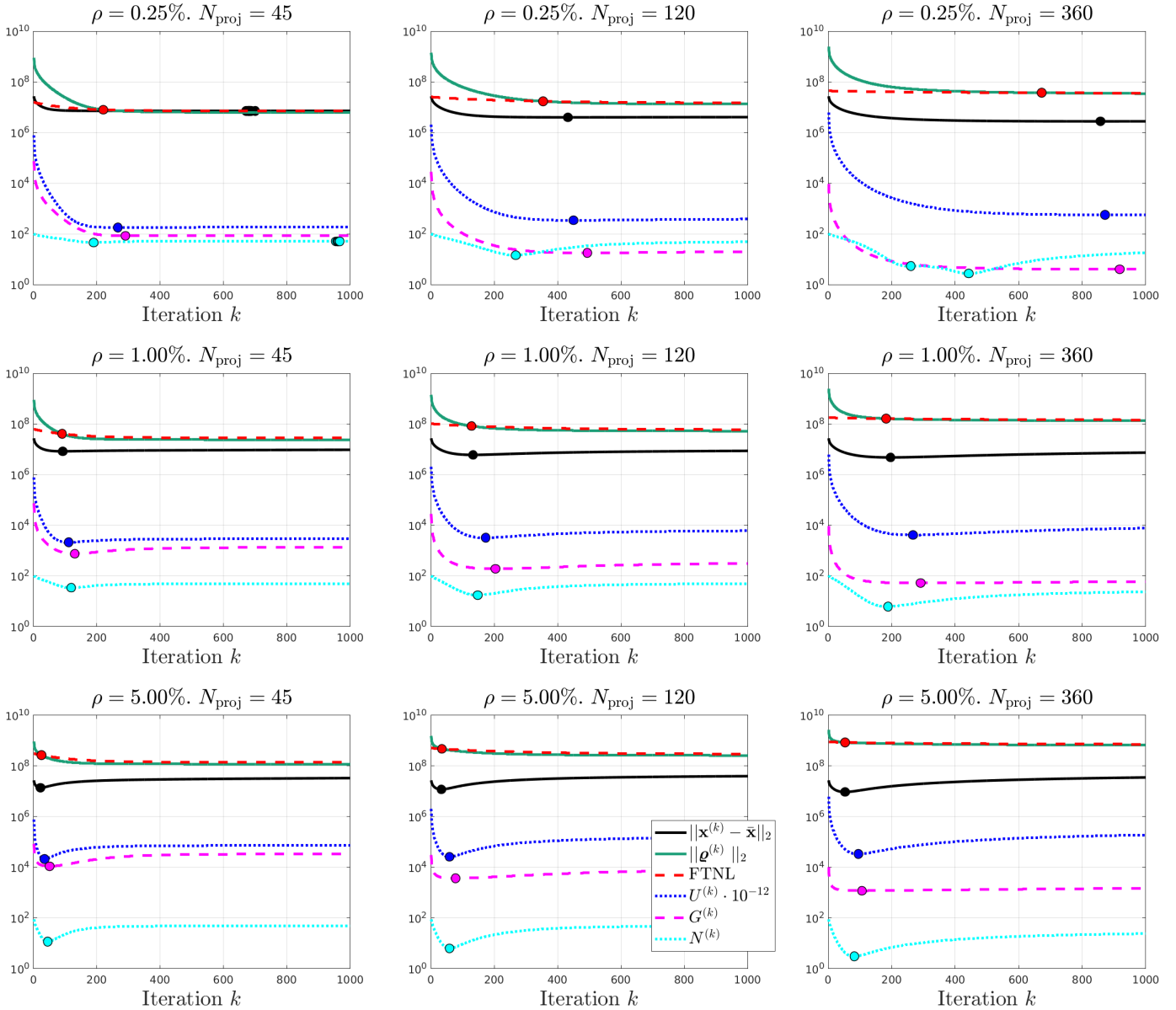


Fig. 9. Illustration of the four different stopping rules for the large-scale example. The filled circles on each curve represent the minimum. Each column has a varying number of projections and each row has a varying amount of noise, as shown in the titles of each subplot.

All images in Fig. 10 are truncated such that their intensities are between 0 and 25,000. Image **a** is the reconstruction after $k = 100$ iteration where it still has a blurred appearance, showing that more iterations are necessary. Images **b** and **c** are the reconstructions at the number of iterations which minimize the reconstruction error and $N^{(k)}$, respectively. The appearance of these reconstructions is very similar, but **c** has a slight increase in noise. The rightmost image **d** is the reconstruction after 1000 iterations where it is noticeable more noisy than **b** and **c**.

V. CONCLUSION

We surveyed several state-of-the-art stopping rules, based on statistical considerations, that are useful for algebraic iterative reconstruction methods in X-ray computed tomography (CT). Common for these stopping rules is that they seek to terminate the iterations at the optimal point where the reconstruction error and the noise error balance each other. They are easy to use and they are also easy to integrate in existing software. We also illustrated the use of two of these methods for a large-scale CT problem related to the study of multiphase flow in chalk. Our numerical experiments show that especially the NCP stopping rule – which is based on statistical properties of

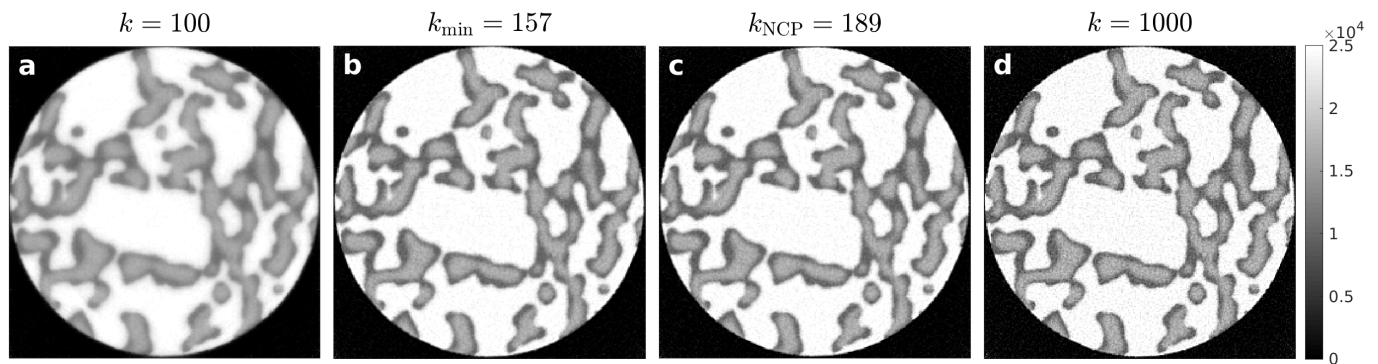


Fig. 10. Illustration of semi-convergence for the large-scale example with 360 projections and noise level $\rho = 1\%$. Results for four different iteration numbers are shown. Image **a** is the reconstruction after 100 iterations. Image **b** is the reconstruction at $k_{\min} = 157$ which is the number of iterations that minimizes the reconstruction error. Image **c** is the reconstruction at $k_{\text{NCP}} = 189$ which is the number of iterations that minimizes $N^{(k)}$. Finally, image **d** is the reconstruction after $k = 1000$ iterations.

the residual and does not depend on knowledge of the noise level – works well for this problem.

ACKNOWLEDGEMENT

We thank the referees for valuable comments.

REFERENCES

- [1] W. van Aarle, W. J. Palenstijn, J. De Beenhouwer, T. Altantzis, S. Bals, K. J. Batenburg, and J. Sijbers, *The ASTRA Toolbox: a platform for advanced algorithm development in electron tomography*, *Ultramicroscopy*, 157 (2015), 35–47.
- [2] W. van Aarle, W. J. Palenstijn, J. Cant, E. Janssens, F. Bleichrodt, A. Dabravolski, J. De Beenhouwer, K. J. Batenburg, and J. Sijbers, *Fast and flexible X-ray tomography using the ASTRA Toolbox*, *Optics Express* (2016), 24(22), 25129–25147.
- [3] A. H. Andersen and A. C. Kak, *Simultaneous algebraic reconstruction technique (SART): a superior implementation of the ART algorithm*, *Ultrasonic Imaging*, 6 (1984), pp. 81–94.
- [4] S. Bruns, S. L. S. Stipp, and H. O. Sørensen, *Statistical representative elementary volumes of porous media determined using greyscale analysis of 3D tomograms*, *Adv. Water Resour.*, 107 (2017), pp. 32–42.
- [5] T. Elfving, T. Nikazad, and C. Popa, *A class of iterative methods: semi-convergence, stopping rules, inconsistency, and constraining*; in Y. Censor, M. Jiang, and G. Wang (Eds.), *Biomedical Mathematics: Promising Directions in Imaging, Therapy Planning, and Inverse Problems*, Medical Physics Publishing, Madison, WI, 2010, pp. 157–184.
- [6] H. W. Engl, M. Hanke, and A. Neubauer, *Regularization of Inverse Problems*, Springer, 1996.
- [7] A. Fakhari, T. Mitchell, C. Leonardi, and D. Bolster, *Improved locality of the phase-field lattice-Boltzmann model for immiscible fluids at high density ratios*, *Physical review. E*, 96(5-1) (2017), 053301.
- [8] A. Fakhari, D. Bolster and L. Luo, *A weighted multiple-relaxation-time lattice Boltzmann method for multiphase flows and its application to partial coalescence cascades*, *J. Computational Physics*, 341 (2017), pp. 22–43.
- [9] A. Girard, *A fast ‘Monte-Carlo cross-validation procedure’ for large least squares problems with noisy data*, *Numer. Math.*, 56 (1989), pp. 1–23.
- [10] G. H. Golub, M. T. Heath, and G. Wahba, *Generalized cross-validation as a method for choosing a good ridge parameter*, *Technometrics*, 21 (1979), pp. 215–223.
- [11] R. Gordon, R. Bender, and G. T. Herman, *Algebraic reconstruction techniques (ART) for three-dimensional electron microscopy and X-ray photography*, *J. Theoretical Biology*, 29 (1970), pp. 471–481.
- [12] P. Gravel, G. Beaudoin and J. A. De Guise, *A method for modeling noise in medical images*, *IEEE Trans. Medical Imaging*, vol. 23 (2004), pp. 1221–1232.
- [13] P. Hall and D. M. Titterton, *Common structure of techniques for choosing smoothing parameters in regression problems*, *J. Royal Stat. Soc.: Series B (Methodological)*, 49 (1987), pp. 184–198.
- [14] P. C. Hansen, J. S. Jørgensen, and M. Saxild-Hansen, *AIR Tools II: algebraic iterative reconstruction methods, improved implementation*, *Numerical Algorithms*, 79 (2018), pp. 107–137.
- [15] P. C. Hansen, J. S. Jørgensen, and W. R. B. Lionheart (Eds.), *Computed Tomography: Algorithms, Insight and Just Enough Theory*, SIAM, Philadelphia, 2021.
- [16] P. C. Hansen, M. E. Kilmer, and R. H. Kjellden, *Exploiting residual information in the parameter choice for discrete ill-posed problems*, *BIT Numerical Mathematics*, 46 (2006), pp. 41–59.
- [17] K. Hahn, H. Schöndube, K. Stierstorfer, J. Hornegger, and F. Noo, *A comparison of linear interpolation models for iterative CT reconstruction by regularization*, *IEEE Trans. Pattern Anal. Machine Intelligence*, 13 (1991), pp. 326–339.
- [18] J. Kay, D. Titterton, J. Brown and A. Thompson, *A Study of Methods of Choosing the Smoothing Parameter in Image Restoration by Regularization*, *IEEE Trans. Pattern Anal. Machine Intelligence*, 13 (1991), pp. 326–339.
- [19] Q. Lin, M. Andrew, W. Thompson, M. J. Blunt and B. Bijeljic, *Optimization of image quality and acquisition time for lab-based X-ray microtomography using an iterative reconstruction algorithm*, *Advances in Water Resources*, 115 (2018), pp. 112–124.
- [20] D. Mütter, H. O. Sørensen, D. Jha, R. Harti, K. N. Dalby, H. Suhonen, R. Feidenhans’l, F. Engström, and S. L. S. Stipp, *Resolution dependence of petrophysical parameters derived from X-ray tomography of chalk*, *Appl. Phys. Lett.*, 105 (2014), 032108.
- [21] F. Natterer, *The Mathematics of Computerized Tomography*, SIAM, Philadelphia, 2001 (reprint).
- [22] W. J. Palenstijn, K. J. Batenburg, and J. Sijbers, *Performance improvements for iterative electron tomography reconstruction using graphics processing units (GPUs)*, *J. Structural Biology*, 176 (2011), pp. 250–253.
- [23] B. W. Rust and D. P. O’Leary, *Residual periodograms for choosing regularization parameters for ill-posed problems*, *Inverse Problems*, 24 (2008), 034005.
- [24] R. J. Santos and Á. R. De Pierro, *A cheaper way to compute generalized cross-validation as a stopping rule for linear stationary iterative methods*, *J. Comput. Graphical Statistics*, 12 (2003), pp. 417–433.
- [25] V. F. Turchin, *Solution of the Fredholm equation of the first kind in a statistical ensemble of smooth functions*, *USSR Comp. Math. and Math. Physics*, 7 (1967), pp. 79–96.
- [26] C. Vogel, *Computational Methods for Inverse Problems*, SIAM, Philadelphia, 2002.
- [27] G. Wahba, *Spline Models for Observational Data*, SIAM, Philadelphia, 1990.